View metadata, citation and similar papers at core.ac.uk
brought to you by CORE
provided by Lirias

Modelling the relationship between CO_2 assimilation and leaf anatomical properties in tomato leaves

Herman N.C. Berghuijs[1], Xinyou Yin[1], Q. Tri Ho[2], Peter E.L. van der Putten[1], Pieter Verboven[2], Moges A. Retta[2], Bart M. Nicolaï[2], Paul C. Struik[1]

[1] Centre for Crop Systems Analysis – Wageningen University and Research Centre, Droevendaalsesteeg 1, 6708 PB Wageningen, The Netherlands

[2] Flanders Center of Postharvest Technology / BIOSYST-MeBioS, Katholieke Universiteit Leuven, Willem de Croylaan 42, B-3001, Leuven, Belgium

e-mail corresponding author: herman.berghuijs@wur.nl

phone no. corresponding author: +31 317485315

Abstract

The CO_2 concentration near Rubisco and, therefore, the rate of CO_2 assimilation, is influenced by both leaf anatomical factors and biochemical processes. Leaf anatomical structures act as physical barriers for CO_2 transport. Biochemical processes add or remove CO_2 along its diffusion pathway through mesophyll. We combined a model that quantifies the diffusive resistance for CO_2 using anatomical properties, a model that partitions this resistance and an extended version of the Farquhar-von Caemmerer-Berry model. We parametrized the model by gas exchange, chlorophyll fluorescence and leaf anatomical measurements from three tomato cultivars. There was generally a good agreement between the predicted and measured light and CO_2 response curves. We did a sensitivity analysis to assess how the rate of CO_2 assimilation responds to changes in various leaf anatomical properties. Next, we conducted a similar analysis for assumed diffusive properties and curvature factors. Some variables (diffusion pathway length in stroma, diffusion coefficient of the stroma, curvature factors) substantially affected the predicted CO_2 assimilation. We recommend more research on the measurements of these variables

and on the development of 2-D and 3-D gas diffusion models, since these do not require the diffusion pathway length in the stroma as predefined parameter.

Key words

Leaf anatomy, photosynthesis, diffusion, mesophyll resistance, mesophyll conductance, C_3

1. Introduction

The biochemical model of Farquhar, von Caemmerer & Berry ('the FvCB model' hereafter) [1] has been widely used to study leaf physiology and to predict leaf photosynthesis under various environmental conditions. This model states that Rubisco-limited and electron-transport-limited rates of CO_2 assimilation depend on the CO_2 partial pressure at the carboxylation sites of Rubisco, C_c (see Table 1 for the definition of symbols used in this study). Assessing C_c is complicated by the mesophyll resistance that substantially constrains CO_2 diffusion from the intercellular airspaces to Rubisco [2-5]

Traditionally, mesophyll resistance r_m is defined as a lumped resistance as:

$$r_m = \frac{(C_i - C_c)}{A_N} \quad (1)$$

where C_i is CO_2 partial pressures in intercellular air-spaces, and A_N is the net rate of CO_2 assimilation. The inverse of mesophyll resistance is mesophyll conductance g_m. Various methods have been developed to estimate r_m indirectly with either chlorophyll fluorescence measurements [6] or ^{13}C isotope discrimination methods [7]. One of the most widely used methods to estimate r_m based on chlorophyll fluorescence measurements is the variable J method [8]. This method, when applied to various C_i or light levels, often shows an initial increase and then decrease of g_m with an increasing C_i or of a continuous increase of g_m with an increasing irradiance I_{inc} [5, 6]. This method is, in principle, only valid for the electron-transport-limited

CO_2 assimilation, and caution is needed when applying it to Rubisco or triose-phosphate-utilization-limited CO_2 assimilation. For example, that the variable J method may underestimate g_m for the low C_i range where CO_2 assimilation is limited by Rubisco activity [9].

Nevertheless, the variability of g_m with C_i in the low C_i range can at least partially be explained by the release of photorespired CO_2 [3, 10]. Photorespiration starts in the stroma with the production of phosphoglycolate through RuBP oxygenation by Rubisco. Phosphoglycolate is converted to glycolate, which is transferred from the stroma to the peroxisomes. In the peroxisome, glycolate is converted to glycine, which is then transferred to a mitochondrion, where glycine is converted to serine and CO_2. Additionally, mitochondrial respiration also releases CO_2. The CO_2 concentration difference between the cytosol and intercellular airspaces is, therefore, smaller than one would expect.

Tholen *et al*. [3] developed a framework to calculate C_c, in which they distinguished the different physical barriers for CO_2 transported from the intercellular air-spaces and CO_2 released from (photo)respiration. They defined r_{diff} as the lumped constant resistance for CO_2 transport due to these barriers in the diffusion pathway of the mesophyll:

$$r_{diff} = r_{wp} + r_{chl} \quad (2)$$

where r_{wp} is defined as the lumped resistance of the cell wall and plasma membrane, and r_{chl} is defined as the lumped diffusive resistance of the chloroplast envelope and the stroma. Based on their framework, C_c can be expressed as:

$$C_c = C_i - r_{diff} A_N - \omega(F + R_d) \quad (3)$$

where $\omega = \frac{r_{chl}}{r_{diff}}$, F and R_d are rates of photorespired and respired CO_2 release, respectively (see also [11])

A number of studies [12-15] have been conducted to investigate the possibility to further partition r_{chl} and r_{wp} and calculate each of these resistances based on leaf

anatomical measurements and assumptions related to the diffusivity for CO_2 of each of these components. These authors found that there was a mismatch between the values for r_m calculated by the variable J method and the values for r_{diff} at ambient CO_2 levels and saturating light. This mismatch may be explained by the framework of Tholen *et al.* [3] that r_m is variable with C_i and that this variability can be associated with the varying levels in the release of photorespired CO_2.

In summary, C_c, and thereby the rate of CO_2 assimilation, is influenced by both leaf anatomical features that act as physical barriers for CO_2 transport and biochemical processes that act as sources and sinks for CO_2 along the CO_2 diffusion pathway in leaves. To the best of our knowledge, there has been no report on predicting the rate of CO_2 assimilation by combining gas exchange, chlorophyll fluorescence, and leaf anatomical measurements. We present a model that combines the model of Tosens *et al*. [13] quantifying r_{diff} from leaf anatomical measurements, the model of Tholen *et al*. [3] partitioning r_{diff}, and an extended version of the original FvCB model [1, 9, 16]. We will use this combined model to investigate to what extent various leaf anatomical traits affect the net rate of CO_2 assimilation at various light and CO_2 levels. We will also use the model for a sensitivity analysis with regard to mesophyll curvature factors and a number of diffusive properties of subcellular components. The results of this analysis demonstrate that some of these parameters substantially affect the net rate of CO_2 assimilation and that their values should therefore not be taken for granted.

2. Materials and methods

2.1 Plant material and growth conditions

We carried out an experiment in an UNIFARM glasshouse of Wageningen University, using three cultivars of tomato (*Solanum lycopersicum* L.): Admiro (Syngenta, The Netherlands), Doloress (De Ruiter Seeds, The Netherlands) and Growdena (Syngenta, The Netherlands). All measurements involved four replicates. In order to spread the measurements over time, seeds were sown in small pots in a staggered way, i.e., on February 18, February 27, March 11, and March 21 of 2013, providing plants of the four replicates, respectively. The plants were grown on substrate blocks saturated with UNIFARM standard tomato nutrient solution (0.854% Calsal^{TM}, 0.15%

Amnitra™, 0.36% Sulfakal™, 0.682% Bascal™, 0.864% Magnesul™ ; all from Yara Benelux, The Netherlands), 0.43% 6 M nitric acid and 0.118% 6 M phosphoric acid. The nutrient solution was supplied by a hydroponic irrigation system. The photoperiod in the greenhouse was 16 h. During day time, supplemental light from 600 W HPS Hortiflux Schréder lamps (Monster, South Holland, The Netherlands, 0.4 lamps m^{-2}) were switched off as soon as the intensity of the global solar radiation dropped below 400 W m^{-2}. Day and night temperatures were kept at 21°C and 16°C (±3°C), respectively. All measurements were carried out on plants that were at least 42 days old, using distal leaflets of the compound leaves that were 15 days old or 25 days old (typically at the fifth and the ninth nodes from the bottom).

2.2 Simultaneous gas exchange and chlorophyll fluorescence measurements

We used the LI-6400XT Portable Photosynthesis System (Li-Cor BioSciences, Lincoln, NE, USA) to simultaneously measure gas exchange and chlorophyll fluorescence. We measured both light and CO_2 response curves. During all measurements, the leaf temperature was kept at 25°C, and the leaf-to-air vapour pressure difference was kept at 1.0-1.6 kPa.

We measured the CO_2 response curves under an incident irradiance (I_{inc}) of 1500 µmol m^{-2} s^{-1} under both 21% and 2% O_2 conditions. The low O_2 condition was created using a gas mixture of 2% O_2 and 98% N_2, and the IRGA calibration was adjusted for the O_2 composition of the gas mixture. The leaflet was consecutively exposed to different levels of CO_2), i.e., 400, 300, 200, 100, 50, 400, 600, 800, 1000, 1200, 1600, and 2000 µmol mol^{-1}. For light response curves, two sets of conditions were used. First, the light response curve was measured when C_{a} was kept constant at 400 µmol mol^{-1} combined with 21% O_2. The light response was also obtained under a non-photorespiratory condition, using 1000 µmol mol^{-1} C_{a} combined with the 2% O_2 gas mixture. During the light response measurements, the leaflet was consecutively exposed to I_{inc} levels of 1500, 1000, 750, 500, 300, 150, 100, 50, and 25 µmol m^{-2} s^{-1}. During all measurements, the plant was allowed to adapt to a new level of CO_2 or light for three minutes, except for the transfer from $C_{\mathrm{a}} = 50\ \mu\mathrm{mol\ mol^{-1}}$ to $C_{\mathrm{a}} = 400\ \mu\mathrm{mol\ mol^{-1}}$. In the latter case, the plant was allowed to adapt for 12 minutes. Preliminary measurements had indicated that such an interval was long enough to obtain steady-state values reliably. Each combination of measured

values for A_N and C_i was corrected for leakage in and out of the cuvette, using thermally killed leaves, as described by Flexas *et al*. [17]

At each light or CO_2 step during the measurements, the steady-state fluorescence F_s was measured. Next, a saturating light pulse (8500 μmol m^{-2} s^{-1}) was applied for less than a second to measure the maximum fluorescence F_m'. These parameters were used to calculate the apparent operating quantum yield of Photosystem II as $\Phi_2 = \frac{F_m' - F_s}{F_m'}$ [18].

2.3 Sample preparation for light and transmission electron microscopy

After the gas exchange and chlorophyll fluorescence measurements, small leaflet samples (5 x 1 mm^2) were cut parallel to the main vein. The samples were vacuum infiltrated in 3% glutaraldehyde in 0.1 M phosphate buffer (pH =7.2), postfixed in 1% osmium tetroxide in 0.1 M phosphate buffer (pH=7.2), and dehydrated in an ethanol series. They were then infiltrated and embedded with Spurr's resin [19]. The samples were put in an oven for 8 h at 70°C for polymerization.

2.4 Light microscopy

Sections of 1 μm thick were cut using an ultramicrotome (Leica EM UC6), and they were stained using methylene blue. The sections were viewed and photographed by a digital inverted microscope (VOS, AMC-3206) at 20x magnification. The microscopic images were digitized using in house MATLAB (The Mathworks Inc, Natick, Massachusetts, USA) software [20]. The digitized images were subsequently loaded into COMSOL 3.5a (COMSOL AB, Stockholm, Sweden). The ratio of the length of the mesophyll exposed to the intercellular airspaces L_m to the length of the section L was calculated using measurements from these images. The exposed mesophyll surface area per unit of leaf area $\frac{S_m}{S}$ was calculated for both the pallisade parenchyma and the spongy parenchyma as:

$$\left(\frac{S_m}{S}\right)_{tissue} = \gamma_{tissue}\left(\frac{L_m}{L}\right)_{tissue} \quad (4)$$

where the subscript tissue indicates either palisade parenchyma or spongy parenchyma tissue, and γ_{tissue} is the curvature factor [21, 22] of the tissue. We adopted γ_{tissue} values for *S. lycopersicum* leaves determined by Galmes *et al*. [23]: 1.497 and 1.281 for the palisade and the spongy parenchyma, respectively.

2.5 Measurements using transmission electron microscopy

Sections of 80 nm thick were cut using an ultramicrotome, stained by lead citrate, and photographed using a transmission electron microscope (TEM Zeiss EM 900). The ratio of the length of chloroplasts exposed to intercellular airspaces L_{c} to the length of exposed mesophyll L_{m} was measured for both the palisade and the spongy parenchyma. The exposed mesophyll surface area covered by chloroplast per unit of leaf area was calculated as:

$$\frac{S_{\mathrm{c}}}{S} = \left(\frac{L_{\mathrm{c}}}{L_{\mathrm{m}}}\right)_{\mathrm{pal}} \left(\frac{S_{\mathrm{m}}}{S}\right)_{\mathrm{pal}} + \left(\frac{L_{\mathrm{c}}}{L_{\mathrm{m}}}\right)_{\mathrm{spo}} \left(\frac{S_{\mathrm{m}}}{S}\right)_{\mathrm{spo}} \quad (5)$$

where the subscripts 'pal' and 'spo' indicate palisade parenchyma and spongy parenchyma, respectively.

Cell wall thickness t_{wall}, cytosol thickness t_{cyt}, and chloroplast stroma thickness t_{str} were measured from these images (Figure 1). The thickness of the cytosol was measured as the average distance between the cell wall and the chloroplast envelope. For each compartment i, the overall thickness t_{i} was calculated as a weighted average between the thickness of compartment i in the palisade parenchyma and the spongy parenchyma:

$$t_{\mathrm{i}} = f_{\mathrm{pal}} t_{\mathrm{i,pal}} + \left(1 - f_{\mathrm{pal}}\right) t_{\mathrm{i,spo}} \quad (6)$$

where f_{pal} is the fraction of exposed mesophyll surface area covered by chloroplast in the palisade parenchyma relative to the total mesophyll surface area covered by chloroplasts.

2.6 Model to calculate the sub-resistances in the mesophyll

Sub-resistance components in the mesophyll, R_{wall}, R_{cyt} and R_{str}, were calculated as described by Niinemets and Reichstein [24] and Tosens *et al*. [13]:

$$R_{\mathrm{i}} = \frac{f_{\mathrm{i}}\, t_{\mathrm{i}}}{p_{\mathrm{eff,i}} \zeta_{\mathrm{i}} D_{\mathrm{CO_2,water}}} \tag{7}$$

where R_{i} is the resistance of component i. t_{i} is the thickness of component i. $D_{\mathrm{CO_2,water}}$ is the diffusion coefficient of CO_2 in pure water at standard pressure and temperature ($D_{\mathrm{CO_2,water}} = 1.79 \cdot 10^{-9}\ \mathrm{m^2\ s^{-1}}$, $P = 101325\ \mathrm{Pa}$, $T = 298.15\ \mathrm{K}$). $p_{\mathrm{eff,i}}$ is the effective porosity for CO_2. ζ_{i} is a reduction factor of the diffusion coefficient of CO_2 relative to that of water due to a higher viscosity. f_{i} is the fraction of the effective diffusion path length in component i. We assumed that ζ_{i} is 1.0 for the cell wall and 0.5 for the cytosol (i.e., $\zeta_{\mathrm{wall}} = 1$, $\zeta_{\mathrm{cyt}} = 0.5$) following Tholen and Zhu [25] and Ho *et al* [26]. It was also assumed that $\zeta_{\mathrm{i}} = 0.5$ for the stroma [26], $f_{\mathrm{str}} = 0.25$ [25], $f_{\mathrm{i}} = 1$ for other components, and $p_{\mathrm{eff,i}} = 1$ for the cytosol and the chloroplast stroma. Finally, we assumed that $p_{\mathrm{eff,i}} = 0.2$ for the cell wall [26, 27]. By applying equation 7, we adopt the commonly used assumption [12-15] that the cell wall thickness measured from transmission electron micrographs is not affected by the dehydration and embedding procedures of the sample preparation [28].

While there are only few data available, reported values of the permeability of the plasma membrane G_{mem} and the chloroplast envelope G_{env} varied considerably [29]. Gutknecht *et al*. [30] found that the permeability of an artificial lipid bilayer membrane that consists of egg lecithin and cholesterol had a permeability of $3.5 \cdot 10^{-3}\ \mathrm{m\ s^{-1}}$. Due to the lack of data, we set G_{mem} equal to this value. Since the chloroplast envelope is a double membrane, we assumed that $G_{\mathrm{env}} = \frac{1}{2} G_{\mathrm{mem}} = 1.75 \cdot 10^{-3}\ \mathrm{m\ s^{-1}}$. G_{mem} lumps the permeability of aquaporins and the bulk plasma membrane [31].

During gas exchange measurements, the rate of photosynthesis is commonly expressed in $\mu\mathrm{mol\ CO_2\ m^{-2}\ leaf\ s^{-1}}$ and the CO_2 level is in $\mu\mathrm{bar\ CO_2}$. Consequently, the unit of diffusive mesophyll resistance $\mathrm{m^2\ leaf\ s\ bar\ CO_2\ mol^{-1}\ CO_2}$, rather than in $\mathrm{s\ m^{-1}}$ for $R_{\mathrm{diff,}}$ resulting from anatomical measurements. We calculated the resistance, expressed in $\mathrm{m^2\ s\ bar\ mol^{-1}}$, from the resistances expressed in $\mathrm{s\ m^{-1}}$. For this purpose,

we used equation 8 to calculate this resistance for the cell wall, plasma membrane and cytosol and equation 9 for the chloroplast envelope and the stroma:

$$r_{i_1} = \left(\frac{S_m}{S}\right)^{-1} \frac{H}{10^5} \frac{f_i\, t_i}{p_{eff,i}\zeta_i D_{CO_2,water}} \quad (8)$$

$$r_{i_2} = \left(\frac{S_c}{S}\right)^{-1} \frac{H}{10^5} \frac{f_i\, t_i}{p_{eff,i}\zeta_i D_{CO_2,water}} \quad (9)$$

where H is Henry's law constant for CO_2 ($H = 2941\ \mathrm{Pa\ m^3\ mol^{-1}}$ at $T = 298.15\ \mathrm{K}$ and standard pressure. 10^5 is a conversion factor to convert Pascals to bars. Its unit is $\mathrm{Pa\ bar^{-1}}$. In equation 8, the subscript 1 refers to the first set of resistance components (i.e., the cell wall, the plasma membrane and the cytosol). The subscript 2 in equation 9 refers to the second set of resistance components (i.e., chloroplast envelope, stroma). We describe the derivation of equations 8 and 9 in Supplementary Material 1. Equation 9 implies that we assume that only chloroplasts that are exposed to the intercellular airspaces affect the net rate of CO_2 assimilation. It is also important to emphasize that we scaled resistances of the cell wall, the plasma membrane and the cytosol with the exposed mesophyll surface area (equation 8) and the resistance of the chloroplast envelope and stroma with the exposed chloroplast surface area. This modification of the original resistance model presented by Tosens *et al*. [13] was necessary to correct for the fact that the mesophyll surface area available for CO_2 uptake is larger than the chloroplast surface area [15].

2.7 Model to calculate ω

The diffusive resistance of the mesophyll r_{diff} (expressed in $\mathrm{m^2\ s\ bar\ mol^{-1}}$) can be considered as a series of sub-resistances. These sub-resistances are resistances of the cell wall, plasma membrane, cytosol, chloroplast envelope, and chloroplast stroma [29]:

$$r_{diff} = r_{wall} + r_{mem} + r_{cyt} + r_{env} + r_{str} \quad (10)$$

where r_{wall}, r_{mem}, r_{cyt}, r_{env} and r_{str} are the resistances of the cell wall, plasma membrane, cytosol, chloroplast envelope and chloroplast stroma [10]. Since we assume that the source for (photo)respired CO_2 release is located halfway in the diffusion pathway in the cytosol (Figure 1), we can calculate ω as:

$$\omega = \frac{r_{\mathrm{env}} + r_{\mathrm{str}} + \frac{1}{2} r_{\mathrm{cyt}}}{r_{\mathrm{diff}}} \tag{11}$$

Note that the diffusive resistance r_{diff} is not the same as the previously defined mesophyll resistance r_{m} [10]. The first one is the sum of the resistances to CO_2 diffusion of all cellular components; the latter one, as defined by equation 1, lumps the effect of r_{diff} and biochemical processes on the overall resistance to CO_2 transport from the intercellular airspaces to Rubisco [10].

2.8 The FvCB model to calculate the rate of photosynthesis

The generic form of the FvCB model is:

$$A_{\mathrm{N}} = \left(1 - \frac{\Gamma^*}{C_{\mathrm{c}}}\right)\left(\frac{C_{\mathrm{c}} X_1}{C_{\mathrm{c}} + X_2}\right) - R_{\mathrm{d}} \tag{12}$$

where R_{d} is day respiration (i.e., the CO_2 release other than by photorespiration), and Γ^* is CO_2 compensation point in the absence of R_{d}. In equation 12, $X_1 = V_{\mathrm{cmax}}$ and $X_2 = K_{\mathrm{mC}}\left(1 + \frac{O}{K_{\mathrm{mO}}}\right)$ if the rate of carboxylation is limited by Rubisco, where V_{cmax} is the maximum rate of carboxylation by Rubisco, K_{mC} and K_{mO} are the Michaelis-Menten kinetic constants of Rubisco for RuBP carboxylation and oxygenation, respectively. If the rate of carboxylation is limited by the rate of electron transport J and this rate is limited by NADPH production rather than ATP production, $X_1 = \frac{1}{4}J$ and $X_2 = 2\Gamma^*$. J can be calculated as:

$$J = \frac{\kappa_{2LL} I_{inc} + J_{max} - \sqrt{(\kappa_{2LL} I_{inc} + J_{max})^2 - 4\theta J_{max} \kappa_{2LL} I_{inc}}}{2\theta} \quad (13)$$

where I_{inc} is the incident irradiance; κ_{2LL} is the efficiency of converting incident irradiance to electron transport under limiting light; J_{max} is the maximum rate of electron transport; and θ is a convexity factor. If the rate of CO_2 assimilation is limited by the rate of triose phosphate utilization T_p [16], $X_1 = 3T_p$ and $X_2 = -\Gamma^*$.

2.9 Parameters of the FvCB model

The CO_2 compensation point Γ^* can be calculated as $\Gamma^* = \frac{0.5O}{S_{C/O}}$, where $S_{C/O}$ is the relative CO_2/O_2 specificity factor of Rubisco. We adopted the values $S_{C/O} = 3.26\ \text{mbar}\ \mu\text{bar}^{-1}$, $K_{mC} = 267\ \mu\text{bar}$ and $K_{mO} = 164\ \text{mbar}$ [26]. The cultivars used in this study were the same as in our study.

The parameter R_d was calculated by linear regression as the intercept of the line $A_N = s(I_{inc}\Phi_2/4) - R_d$ as described by Yin *et al*. [9], using data of the electron-transport-limited range of the $A - I_{inc}$ ($I_{inc} \leq 200\ \mu\text{mol m}^{-2}\ \text{s}^{-1}$) curve under non-photorespiratory condition conditions. The slope *s* of this linear regression was used as a calibration factor to calculate values of electron transport rate: $J = sI_{inc}\Phi_2$ [9]. We estimated the efficiency of photosystem II (Φ_{2LL}) according to the method described by Yin *et al* [9]. We calculated κ_{2LL} as $\kappa_{2LL} = s\Phi_{2LL}$. We then used the calculated values for κ_{2LL} as an input to estimate J_{max} and θ for each leaf type by fitting the calculated J ($J = sI_{inc}\Phi_2$) to equation 13.

2.10 Coupling of the FvCB model with the gas diffusion model

Combining the FvCB model, equation 12, with the CO_2 diffusion model, equation 3, results in:

$$A_N = \frac{-\mathcal{B} - \sqrt{\mathcal{B}^2 - 4\mathcal{A}\mathcal{C}}}{2\mathcal{A}} \quad (14)$$

with

$$\mathcal{A} = X_2 + \Gamma^*(1-\omega) \quad (15)$$

$$\mathcal{B} = -\left\{[X_2 + \Gamma^*(1-\omega)](X_1 - R_\mathrm{d}) - \omega(R_\mathrm{d}X_2 + \Gamma^* X_1) + (C_\mathrm{i} + X_2)\left[\frac{1}{r_\mathrm{diff}}(X_2 + \Gamma^*)\right]\right\} \quad (16)$$

$$\mathcal{C} = -\omega(R_\mathrm{d}X_2 + \Gamma^* X_1)(X_1 - R_\mathrm{d}) + \frac{1}{r_\mathrm{diff}}(X_2 + \Gamma^*)[X_1(C_\mathrm{i} - \Gamma^*) - R_\mathrm{d}(C_\mathrm{i} + X_2)] \quad (17)$$

Equations 14-17 were applied to calculate the net rate of CO_2 assimilation limited by Rubisco ($A_{\mathrm{N,c}}$) or by electron transport ($A_{\mathrm{N,j}}$). We calculated the net rate of CO_2 assimilation limited by triose phosphate utilization ($A_{\mathrm{N,p}}$) as $A_{\mathrm{N,p}} = 3T_\mathrm{p} - R_\mathrm{d}$. The actual net rate of CO_2 assimilation was the minimum of these three potential rates. This model was used to estimate V_{cmax} and T_p, using already estimated or measured parameter values as input.

2.11 Relationship between C_i and I_inc

In order to interpolate the rate of photosynthesis for light levels that were not measured, it is necessary to know C_i. An empirical relationship between C_i and I_inc was found by fitting data for C_i and I_inc to a power law:

$$C_\mathrm{i} = C_{\mathrm{i}0} {I_\mathrm{inc}}^{q} \quad (18)$$

Next, we simulated two additional light response curves for 25-day-old Admiro leaves for both ambient and low oxygen levels. In each of these curves, C_i is fixed to the average of all C_i measurements in the light response curve measurements rather than that calculated by equation 18.

2.12 Sensitivity analysis

We simulated light and CO_2 response curves for 15-day-old Admiro leaves at ambient O_2 levels using different assumed parameter values (γ_{pal}, γ_{spo}, $p_{\mathrm{eff,wall}}$, G_{mem}, ζ_{cyt}, G_{env}, f_{str} and ζ_{str}) and measured leaf anatomical properties (t_{wall}, t_{cyt}, t_{str}, $\frac{L_\mathrm{m}}{L}$, $\frac{L_\mathrm{c}}{L_\mathrm{m}}$). Each time, one of these properties was changed by -25%, and +25%, respectively, while keeping the remaining variables at their default value.

3. Results

3.1 Leaf anatomical measurements

Table 2 shows the ratio of the measured length of mesophyll exposed to the intercellular airspaces to the total width of the section $\frac{L_\mathrm{m}}{L}$. The values of $\frac{L_\mathrm{m}}{L}$ varied between 4.87 and 6.01 in the palisade parenchyma and between 6.28 and 7.06 in the spongy parenchyma. The ratio of the length of chloroplasts exposed to the intercellular airspaces to the length of exposed mesophyll $\frac{L_\mathrm{c}}{L_\mathrm{m}}$ was also measured.

We calculated values for $\frac{S_\mathrm{c}}{S}$ for the palisade parenchyma, the spongy parenchyma and the whole mesophyll (Table 2). The values for $\frac{S_\mathrm{c}}{S}$ in the mesophyll ranged from 14.3 to 16.4.

The thicknesses of the mesophyll components were measured for each cultivar, leaf age, and tissue type. Table 3 shows the weighted average thicknesses of the mesophyll components (see equation 6). The average cell wall thickness ranged from 0.089 µm to 0.208 µm. The weighted average thickness of the cytosol ranged from 0.172 µm to 0.492 µm and of the stroma from 2.035 µm to 2.708 µm.

3.2 Determination of R_i, r_diff, and ω

The thicknesses of the cell wall, cytosol and stroma and the assumed values of p_eff, f_i and ζ_i were used to calculate the resistance for each component in the mesophyll (R_i; see eqn 7). Since we assumed that the permeability of the membranes $G_\mathrm{mem} = G_\mathrm{env} = 3.5 \cdot 10^{-3}\ \mathrm{m\ s^{-1}}$ was the same for all leaf types, their resistances were the same as well. Table S1 shows the values of these partitioned resistances. We used equation 8 and 9 to convert the unit for the resistance of each component from $\mathrm{s\ m^{-1}}$ to $\mathrm{m^2\ s\ bar\ mol^{-1}}$. Table S2 shows the values of these partitioned resistances. We applied equation 10 and 11 to calculate r_diff and ω. Table 4 shows the calculated values of these variables. The values for ω varied between 0.62 and 0.67 (Table 4). For all cultivars, ω was higher for 15-day-old leaves than for 25-day-old leaves. The values

for r_{diff} varied between 3.85 and 5.09 $\mathrm{m^2\ s\ bar\ mol^{-1}}$. For all cultivars r_{diff} was higher for 15-day-old leaves than for 25-day-old leaves.

3.3 Parameters relationship between I_{inc} and C_{i}

Table S3 displays the estimates for C_{i0} and q that describe the relationship between I_{inc} and C_{i}. At $O = 210\ \mathrm{mbar}$ and $C_{\mathrm{a}} = 400\ \mu\mathrm{bar}$, C_{i0} varies between 617 and 862 $\mu\mathrm{bar}$ and q varies between -0.126 and -0.218. At $O = 20\ \mathrm{mbar}$ and $C_{\mathrm{a}} = 1000\ \mu\mathrm{bar}$, C_{i0} varies between 1224 $\mu\mathrm{bar}$ and 1949 $\mu\mathrm{bar}$ and q varies between -0.070 and -0.204 . Figure S2 shows the simulated and the measured relationship between I_{inc} and C_i.

3.4 Estimation of photosynthetic parameters

The estimated values for R_{d} varied from 1.35 $\mu\mathrm{mol\ m^{-2}\ s^{-1}}$ to 2.65 $\mu\mathrm{mol\ m^{-2}\ s^{-1}}$, and the values for s varied from 0.413 to 0.529 (Table S4).

For all cultivars and leaf ages, Φ_{2LL} was larger at $O = 210\ \mathrm{mbar}$ than at $O = 20\ \mathrm{mbar}$ (Table S5). The estimated values for J_{max} ranged from 157.1 to 263.7 $\mu\mathrm{mol\ m^{-2}\ s^{-1}}$ at $O = 210\ \mathrm{mbar}$ and $C_{\mathrm{a}} = 400\ \mu\mathrm{bar}$, and from 149.8 to 179.8 $\mu\mathrm{mol\ m^{-2}\ s^{-1}}$ at $O = 20\ \mathrm{mbar}$ and $C_{\mathrm{a}} = 1000\ \mu\mathrm{bar}$ (Table S5). The values for J_{max} were higher in 15-day-old leaves than in 25-day-old leaves only under $O = 20\ \mathrm{mbar}$. The values for θ ranged from 0.760 to 0.851 (Table S5). Finally, Table S5 shows the calculated values of κ_{2LL} (as $\kappa_{\mathrm{2LL}} = s\Phi_{\mathrm{2LL}}$).

The estimates for V_{cmax} and T_{p} are shown in Table S6. The estimates for V_{cmax} vary between 219 $\mu\mathrm{mol\ m^{-2}\ s^{-1}}$ and 274 $\mu\mathrm{mol\ m^{-2}\ s^{-1}}$. The standard errors of the estimates of V_{cmax} are relatively high. This may either reflect that the number of data points in the Rubisco-limited range was limited, or that anatomical data on r_{diff} and ω may not match the curvature of the initial part of $A - C_{\mathrm{i}}$ curves from gas exchange measurements, or both. The estimates for T_{p} vary between 12.6 $\mu\mathrm{mol\ m^{-2}\ s^{-1}}$ and 13.6 $\mu\mathrm{mol\ m^{-2}\ s^{-1}}$. There was no triose-phosphate-limitation for 25-day-old Doloress leaves.

3.5 Comparison of measured and simulated CO_2 and light response curves

Figure 2 displays both the measured and modelled CO_2 response curve for each leaf type and oxygen level. Figure 3 shows both the measured and simulated light response curves for each leaf type and condition (either $O = 210\,\mathrm{mbar}$ and $C_\mathrm{a} = 400\,\mu\mathrm{bar}$ or $O = 20\,\mathrm{mbar}$ and $C_\mathrm{a} = 1000\,\mu\mathrm{bar}$). In general, the model reasonably fitted to the data, although the model underestimates the net rate of CO_2 assimilation at high CO_2 and light levels for 25-day-old Doloress leaves except for the light response curves measured at ambient O_2 and CO_2 levels. The underestimation of the net CO_2 assimilation rate may be caused by the estimate of s (Table S4). The estimate of s for 25-day-old Doloress leaves ($s = 0.413$) and, thereby, the calculated value of $\kappa_{2\mathrm{LL}}$ ($\kappa_{2\mathrm{LL}} = s\Phi_{2LL}$) are considerably lower than in the other five leaf types (between 0.462 and 0.529). This may have resulted in an underestimation of J_max, which may explain the mediocre fit of the model with the data at high CO_2 and light levels. This suggests that the s estimate for this leaf type from the lower part of the $A - I_\mathrm{inc}$ curve under the non-photorespiratory condition does not represent the situation across the high light and CO_2 ranges. The model also predicted that the rate of CO_2 assimilation somewhat decreased with increased irradiances. This contradicts the measurements that did not show this trend.

3.6 Sensitivity analysis of CO_2 response curves

The left panels of figures 4-7 display simulated $A - C_\mathrm{i}$ curves for each leaf type at ambient oxygen and $I_\mathrm{inc} = 1500\,\mu\mathrm{mol\,m^{-2}\,s^{-1}}$ In each simulated curve, one of the model parameters was either increased or decreased by 25%, while the remaining parameter values were kept at their default values. Not surprisingly, in the parts of the simulated curves limited by triose-phosphate-utilization, the rate of CO_2 assimilation was the same for any parameter value. In the remaining parts of the simulated curves, the response of A_N to 25% changes in any parameter value shows the following pattern. Initially, at low CO_2 levels the difference between the predicted rate of CO_2 assimilation with an adjusted parameter value and the rate of CO_2 assimilation with the default parameter value increased with C_i. At higher CO_2 levels, this difference decreased with C_i. The predicted rate of CO_2 assimilation increased with $\frac{L_\mathrm{m}}{L}$, $\frac{L_\mathrm{c}}{L_\mathrm{m}}$ p_eff, G_mem, ζ_cyt, G_env, ζ_str, γ_pal and γ_spo in the non-triose-phosphate-utilization-limited parts of the simulated curves. In contrast, the predicted rate of CO_2 assimilation decreased with t_wall, t_cyt, t_str and f_str. We did not show the simulated $A - C_\mathrm{i}$ curves for 25% changes of t_wall, t_cyt, p_eff, and $G_\mathrm{mem}$because 25% change in

these parameters only resulted in a small response of the net rate of CO_2 assimilation, which can hardly be made visible in these figures. We did not increase $\frac{L_c}{L_m}$ by 25%, because the value of this parameter cannot be larger than 1.

Table 5 shows for the sensitivity analysis of each parameter what the maximum difference in the predicted A_N between changed parameter values and default parameter values was. CO_2 assimilation was most sensitive to 25% changes in the values of $\frac{L_m}{L}$ and $\frac{L_c}{L_m}$.

3.7 Sensitivity analysis of light response curves

The right panels of Figures 4-6 display simulated $A - I_{inc}$ curves for each leaf type at ambient CO_2 and O_2 levels, when one of the model parameters was either increased or decreased by 25% while the remaining parameter values were kept at their default values. The response of CO_2 assimilation to 25% changes in any of the parameter values showed the following pattern. The difference between A_N predicted using an adjusted parameter value and A_N using the default value increased with I_{inc}. Table 6 shows the maximum difference between the simulated value of A_N for default parameters values and for parameter values for which one is 25% increased or decreased. CO_2 assimilation was most sensitive to 25% changes in the values of $\frac{L_m}{L}$ and $\frac{L_c}{L_m}$. We did not show the simulated $A - I_{inc}$ curves for 25% changes of t_{wall}, t_{cyt}, ζ_{cyt}, p_{eff}, and G_{mem}, because 25% change in these parameters only resulted in a small response of the net rate of CO_2 assimilation, which can hardly be made visible in these figures. We found that setting $\frac{L_c}{L_m}$ to 1 (Figure 4) for both the palisade and the spongy parenchyma results in an increase in the net rate of CO_2 assimilation of 0.87 $\mu mol\ m^{-2}\ s^{-1}$ at 1500 $\mu mol\ m^{-2}\ s^{-1}$.

4 Discussion

In this study, we combined the leaf anatomical model described by Tosens *et al*. [13] and the biochemical models for C_3 photosynthesis described by Farquhar *et al*. [1] and Yin *et al*. [9] and the CO_2 diffusion model of Tholen *et al*. [3]. We used this

combined model to directly calculate the rate of CO_2 assimilation based on a combination of leaf anatomical and photosynthetic parameters. The model generally agreed well with the data, although the net rate of CO_2 assimilation tended to slightly decrease as the light intensity increased at high light levels. We used the model to simulate how the net rate of CO_2 assimilation responds to changes in thickness of mesophyll subcellular components, exposed mesophyll and chloroplast surface areas, palisade and spongy mesophyll curvature factors, and a range of assumed diffusive properties. Although there were large differences between the extent of the response of the rate of CO_2 assimilation to each parameter, we found two overall trends. At low C_i levels, the increase or decrease of the rate of CO_2 assimilation in response to changing a parameter value initially increased with C_i. For higher CO_2 levels, it later decreased with C_i. Second, this increase or decrease increased with I_inc. These two findings have important consequences. Tholen *et al*. [32] reviewed the progress of genetic engineering of specific leaf anatomical traits to improve the efficiency of CO_2 transport in leaves. The results of our sensitivity analysis indicate that the potential gain of photosynthetic capacity by changing leaf anatomical traits may strongly depend on the CO_2 and light levels in the environments of such an enhanced plant.

Since this is the first study that uses a resistance model to directly calculate the net CO_2 assimilation rate based on leaf anatomical measurements, we found it was necessary to compare our results with the overall mesophyll conductances calculated in earlier studies. Therefore, we first used our current model to calculate C_c by combining equations 3 and 12. Second, we calculated the overall mesophyll conductance as $g_\mathrm{m} = \frac{(C_\mathrm{i} - C_\mathrm{c})}{A_\mathrm{N}}$ at $I_\mathrm{inc} = 1500\ \mu\mathrm{mol\ m^{-2}\ s^{-1}}$ and ambient O_2 and CO_2. The results are shown in Table S6. According to our analysis, g_m varies between 0.085 mol m^{-2} s^{-1} bar^{-1} and 0.223 mol m^{-2} s^{-1} bar^{-1}. There is quite some variation in g_m for tomato. Galmès *et* al. [23] calculated the overall mesophyll conductance (g_m) by the variable J method [8] in a range of Mediterranean accessions grown under well watered conditions. They reported that g_m varies between 0.170 mol m^{-2} s^{-1} bar^{-1} and 0.289 mol m^{-2} s^{-1} bar^{-1} under saturating light and ambient CO_2. We also used the variable J method to calculate g_m from another data-set consisting of combined gas exchange and chlorophyll fluorescence measurements on the same cultivars as the ones used in this study [26]. We found that g_m varied between 0.0718 mol m^{-2} s^{-1} bar^{-1} and 0.246 mol m^{-2} s^{-1} bar^{-1}. The values for g_m, calculated by the model

presented in the current study, are within the range of the values determined from these earlier studies.

The results of the sensitivity analysis model indicate that $\frac{S_m}{S}$ and $\frac{S_c}{S_m}$ are the most important anatomical properties in determining photosynthetic capacity. The most important assumed diffusive properties are G_{mem}, ζ_{str} and f_{str}. The results of our sensitivity analysis showed that changing t_{wall} had less influence on the net CO_2 assimilation rate. This may contradict with the results from Tosens *et al*. [13], which suggest that the cell wall determines more than half of r_{diff}. This may be explained by the fact that the range of t_{wall} for the species used in their study was considerably higher (from 252 nm to 420 nm) than in our study (119 nm to 193 nm). It may also be explained by the value of p_{eff} that we chose, which is higher than that assumed in their study. It is important to emphasize that assumptions on the diffusive properties of the different components of the liquid phase of the mesophyll may affect the calculated value for r_{diff}. These properties are hard to measure and uncertain [29]. Evans *et al*. [29] argued that the value of $p_{eff,wall}$ varies between 0.02 and 0.2. In our model, we assumed that $p_{eff,wall} = 0.2$ and $\zeta_{str} = 0.5$. The latter value is considerably higher than the ones applied in a number of other studies [12, 13, 15, 24]. These authors all assumed that the reduction factor of the diffusion coefficient for CO_2 in the stroma relative to water is equal the ratio of the effective water self-diffusion coefficients in duck embryo and in water [24]. However, the application of their assumed values of ζ_{str} resulted in considerable underestimations of the rate of CO_2 assimilation at high light or low CO_2 levels (Figure S1a-b) in 15-day-old Admiro leaves at both $p_{eff,wall}$=0.02 and $p_{eff,wall} = 0.2$. When we changed ζ_{str} from 0.294 to 0.5, while keeping $p_{eff,wall}$at 0.02, the underestimation of the rate of CO_2 assimilation became considerably less. We conclude that the rate of CO_2 assimilation is sensitive to the diffusion coefficient of the stroma for the whole range of biologically relevant values of p_{eff} ([29]). This makes the assumed diffusive properties that make up this diffusion coefficient; f_{str} and ζ_{str}, important parameters. In the resistance model described by Tosens *et al*. [13], it is assumed that the diffusion path length of CO_2 molecules in the chloroplasts is half the total thickness of the chloroplasts ($f_{str} = 0.5$). In contrast, results from CO_2 diffusion simulations in a virtual 3D cell [25] suggest that $f_{str} = 0.25$ at saturating light and a CO_2 intercellular partial pressure of 30 Pa. In our model, we adopted the latter value as the default value for f_{str}. Figures S1c-d show $A - C_i$ curves and $A - I_{inc}$ curves for different combinations of values for $p_{eff,wall}$ and ζ_{str} if we would have assumed that $f_{str} = 0.5$, as suggested by Tosens *et al*. [13].

These curves show that the net rate of CO_2 assimilation at 21% O_2 is underestimated, even if we assume high values for ζ_{str} and p_{eff}. This analysis shows that f_{str} and, therefore, the length of the diffusion pathway, is an important parameter to determine the net rate of CO_2 assimilation. Additionally, the diffusion pathway length of CO_2 in the stroma may depend on the CO_2 sink, i.e. RuBP carboxylation, which depends on C_{c} and I_{inc}. This suggests that f_{str} may vary with environmental conditions. We recommend more research on both the diffusion coefficient for CO_2 and the length of the diffusion pathway in the stroma. The uncertainty of the CO_2 diffusion pathway length can be tackled by the use of 2D [33] or 3D models [25, 26, 34, 35] to model CO_2 transport in mesophyll cells, since these models do not require a predefined value for f_{str}.

Other assumed diffusive properties may also be important. Uehlein *et al*. [36] attempted to measure the permeability of the plasma membranes and the chloroplast envelopes for CO_2 in *Nicotiana tabacum* L. from isolated vesicles from these membranes, and found that these permeability values were $8 \cdot 10^{-5}\ \mathrm{m\ s^{-1}}$ and $2 \cdot 10^{-5}\ \mathrm{m\ s^{-1}}$, respectively. However, these methods have a number of shortcomings which may result in large underestimation of the permeability values of membranes [25]. Gutknecht *et al*. [30] estimated that the permeability of lipid bilayers was $3.5 \cdot 10^{-3}\ \mathrm{m\ s^{-1}}$ based on $^{14}CO_2$ flux measurements through artificial lipid bilayer membranes that consisted of egg lecithin and cholesterol. Due to a lack of data, we adopted this value for G_{mem} and assumed that $G_{\mathrm{env}} = \frac{1}{2} G_{\mathrm{mem}}$, because the chloroplast envelope is a double membrane. We also assumed that both G_{mem} and G_{env} are parallel resistances that lump the permeabilities of aquaporines and the remaining parts of the membranes [31].

Our model requires the calculation of $\frac{S_{\mathrm{m}}}{S}$. Evans *et al* [22] described how $\frac{S_{\mathrm{m}}}{S}$ can be calculated, after the determination of curvature factors [21] from a combination of paradermal and transversal leaf sections. In our measurements, no paradermal sections were collected. We adopted the curvature factors γ_{pal} and γ_{spo} for the palisade and the spongy parenchyma of tomato from a previous study [23]. We showed in our sensitivity analysis that the simulated rate of photosynthesis was sensitive to changes of γ_{pal} and γ_{spo}. Tomas *et al*. [15] measured both curvature factors for 15 different species with a wide range of foliage characteristics. They found that γ_{pal} varied from 1.4 to 1.5 and γ_{spo} from 1.16 to 1.4. Combined with the results of our sensitivity analysis, this suggests that it is important to measure this

parameter for unknown species, if one wants to relate $\frac{S_m}{S}$ to the photosynthetic capacity of these leaves. The need for a method to calculate curvature factors to calculate $\frac{S_m}{S}$ can be circumvented by measuring exposed mesophyll surfaces directly from 3D leaf images. One way to obtain these images is to use synchrotron radiation X-ray tomography. Verboven *et al*. [37] used this technique to measure $\frac{S_m}{S}$ directly and also validated the method of Thain [21] by determining the curvature factors from 2D sections of the tomography. An advantage of this method over the method of Thain [21] is that it does not require a fixed orientation of all samples and that it requires fewer samples. This technique or other 3-D imaging techniques may be used in future research to determine $\frac{S_m}{S}$ as an alternative to the method of Thain [21].

Both in the framework of Tholen *et al.* [3] and in our model, it is assumed that all CO_2 produced by normal respiration and photorespiration is released by mitochondria in the cytosol between the plasma membrane and the chloroplast envelope. It is not clear where the mitochondria are located in the cytosol (either between chloroplast envelope and plasma membrane, between chloroplast envelope and tonoplast, or both), but their location may strongly affect the reassimilation of (photo)respired CO_2. Tholen *et* al. [3] pointed out that if the mitochondria are located between the tonoplast and the chloroplast envelope, the effect of (photo)respiration on mesophyll resistance may be small or even insignificant [10]. We observed that the model predicts a slightly decreasing rate of CO_2 assimilation with increasing I_{inc} at high light levels and ambient oxygen and CO_2 levels in 25-day-old leaves (Fig. 3). In contrast, we did not see this behaviour at non-photorespiratory conditions ($C_a = 1000\ \mu bar$, $O = 20\ mbar$). Our assumptions about the location of mitochondria may partly explain this behaviour. If the predicted rate of photorespiration is high, there is a considerable release of CO_2 in the cytosol. This CO_2 release will decrease the concentration difference between the cytosol and the intercellular air spaces and, thereby, will decrease the predicted CO2 flux over the plasma membrane and the cell wall. An alternative explanation is that we described the relationship between I_{inc} and C_i by equation 18 (Figure S2). This empirical relationship predicts that C_i can decrease with I_{inc}, a commonly observed trend that is possibly a consequence of regulation set by stomatal resistance. This decrease in C_i means an increase in the rate of photorespiration under these high light conditions. If we set ω equal to 0, we implicitly assume that (photo)respired CO_2 release and CO_2 consumption by photosynthesis take place in the same compartment (i.e. the stroma). In this specific

case, there is no longer a CO_2 source halfway the diffusion path in the cytosol, so any decrease of net CO_2 assimilation can fully be explained by equation 18. Figure S3 shows a simulated light response curve for 25-day-old Growdena leaves for $\omega = 0$. The decrease of the net CO_2 assimilation rate with I_{inc} (Figure S3) is strongly reduced compared to assuming the default value for ω. This suggests that the empirical relationship between C_{i} and I_{inc} used in this model can only partly explain the simulated decrease of the CO_2 assimilation rate with I_{inc}. We therefore suspect that at least part of the mitochondria may be located between the chloroplast envelope and the tonoplast. In future studies, the effect of different locations of mitochondria may be better studied in 2D [33] or 3D modelling approaches [25, 26, 34, 35]. These models are much more flexible in terms of changing the modelled leaf structure than resistance models [38] like the one used in this study.

It has been frequently debated whether or not carbonic anhydrases (CA) facilitate CO_2 transport in the mesophyll [29, 39, 40]. Results from studies on *Nicotiana tabacum* mutants, in which CA activity was knocked out by antisense RNA, suggest that the rate of CO_2 assimilation is not affected at ambient CO_2 at both saturating light [41] and lower light (150 – 400 µmol m^{-2} s^{-1}) conditions [42] compared with wild type individuals. On the other hand, Gillon and Yakir [43] suggest that CA activity in the chloroplasts has an influence on the CO_2 assimilation rate in species with high $\frac{r_{\mathrm{wp}}}{r_{\mathrm{chl}}}$ ratios like *Quercus robur* (oak) where they found that $\frac{r_{\mathrm{wp}}}{r_{\mathrm{chl}}} = 3.2$. Our anatomical data and assumed diffusive properties show for different cultivars and ages after emergence that $\frac{r_{\mathrm{wp}}}{r_{\mathrm{chl}}}$ is between 0.48 and 0.62. These values are all even smaller than the ratio $\frac{r_{\mathrm{wp}}}{r_{\mathrm{chl}}} = 0.8$ found in *N. tabacum*, in which no significant reduction of the net rate of CO_2 assimilation was found in several studies [41-43] . We therefore surmise that CA facilitation only has a limited effect on the net rate of CO_2 assimilation in the leaves used in this study and, therefore, we did not model CA facilitation explicitly. Evans *et al*. [29] argued that CA facilitation mainly takes place in the cytosol and the stroma. Therefore, if CA facilitation does occur, its effect on CO_2 transport is lumped in the parameters ζ_{cyt} and ζ_{str} of our model.

To the best of our knowledge, this study presents the first attempt to quantify the rate of CO_2 assimilation by combining a resistance model based on leaf anatomical measurements and diffusive properties, and simultaneous gas exchange and chlorophyll fluorescence measurements. This approach can potentially contribute a lot to understand the relationship between leaf anatomy and leaf photosynthesis, but

it relies on a number of unknown diffusive properties and curvature factors. We demonstrated that the diffusion path length for CO_2 and its diffusion coefficient in the stroma, and the curvature factors of palisade and spongy parenchyma substantially affect the predicted net CO_2 assimilation rate. We therefore recommend more research to measure these parameters and to develop sophisticated 2-D or 3-D models that do not require the diffusion path length of the stroma as an input factor.

Acknowledgements

We thank Tiny Franssen-Verheijen (Wageningen University, Laboratory of Virology) and Norbert de Ruiter (Wageningen University, Laboratory of Cell Biology) for advice and technical support during sample preparation, An Vandoren (KU Leuven, Laboratory of Socioecology and Social Evolution) for cutting the sections of the light and electron microscopy samples, Johan Billen (KU Leuven, Laboratory of Socioecology and Social Evolution) for granting access to a transmission electron microscope and for support in making TEM images, and all employees of UNIFARM (Wageningen University) for assisting in cultivating the plants used in this study. Wageningen based authors thank the BioSolar Cells programme (project C3B3) for financial support. Leuven based authors thank the Research Council of the KU Leuven (project OT 12/055) for financial support.

References

[1] G.D. Farquhar, S.V. Caemmerer, J.A. Berry, A biochemical-model of photosynthetic CO_2 assimilation in leaves of C_3 species, Planta, 149 (1980) 78-90.

[2] Y. Sun, L.H. Gu, R.E. Dickinson, S.G. Pallardy, J. Baker, Y.H. Cao, F.M. DaMatta, X.J. Dong, D. Ellsworth, D. Van Goethem, A.M. Jensen, B.E. Law, R. Loos, S.C.V. Martins, R.J. Norby, J. Warren, D. Weston, K. Winter, Asymmetrical effects of mesophyll conductance on fundamental photosynthetic parameters and their relationships estimated from leaf gas exchange measurements, Plant Cell Environ, 37 (2014) 978-994.

[3] D. Tholen, G. Ethier, B. Genty, S. Pepin, X.G. Zhu, Variable mesophyll conductance revisited: theoretical background and experimental implications, Plant Cell Environ, 35 (2012) 2087-2103.

[4] U. Niinemets, A. Diaz-Espejo, J. Flexas, J. Galmes, C.R. Warren, Importance of mesophyll diffusion conductance in estimation of plant photosynthesis in the field, J Exp Bot, 60 (2009) 2271-2282.

[5] J. Flexas, M. Ribas-Carbo, A. Diaz-Espejo, J. Galmes, H. Medrano, Mesophyll conductance to CO_2: current knowledge and future prospects, Plant Cell Environ, 31 (2008) 602-621.

[6] X. Yin, P.C. Struik, Theoretical reconsiderations when estimating the mesophyll conductance to CO_2 diffusion in leaves of C_3 plants by analysis of combined gas exchange and chlorophyll fluorescence measurements, Plant Cell Environ, 32 (2009) 1513-1524.

[7] T.L. Pons, J. Flexas, S. von Caemmerer, J.R. Evans, B. Genty, M. Ribas-Carbo, E. Brugnoli, Estimating mesophyll conductance to CO_2: methodology, potential errors, and recommendations, J Exp Bot, 60 (2009) 2217-2234.

[8] P.C. Harley, F. Loreto, G. Dimarco, T.D. Sharkey, Theoretical considerations when estimating the mesophyll conductance to CO_2 flux by analysis of the response of photosynthesis to CO_2, Plant Physiol, 98 (1992) 1429-1436.

[9] X. Yin, P.C. Struik, P. Romero, J. Harbinson, J.B. Evers, P.E.L. Van Der Putten, J. Vos, Using combined measurements of gas exchange and chlorophyll fluorescence to estimate parameters of a biochemical C_3 photosynthesis model: a critical appraisal and a new integrated approach applied to leaves in a wheat (*Triticum aestivum*) canopy, Plant Cell Environ, 32 (2009) 448-464.

[10] D. Tholen, G. Ethier, B. Genty, Mesophyll conductance with a twist, Plant Cell Environ, 37 (2014) 2456-2458.

[11] F.J. Cano, R. Lopez, C.R. Warren, Implications of the mesophyll conductance to CO2 for photosynthesis and water-use efficiency during long-term water stress and recovery in two contrasting *Eucalyptus species*, Plant Cell Environ, 37 (2014) 2470-2490.

[12] J.J. Peguero-Pina, J. Flexas, J. Galmes, U. Niinemets, D. Sancho-Knapik, G. Barredo, D. Villarroya, E. Gil-Pelegrin, Leaf anatomical properties in relation to differences in mesophyll conductance to CO_2 and photosynthesis in two related Mediterranean *Abies* species, Plant Cell Environ, 35 (2012) 2121-2129.

[13] T. Tosens, U. Niinemets, M. Westoby, I.J. Wright, Anatomical basis of variation in mesophyll resistance in eastern Australian sclerophylls: news of a long and winding path, J Exp Bot, 63 (2012) 5105-5119.

[14] T. Tosens, U. Niinemets, V. Vislap, H. Eichelmann, P.C. Diez, Developmental changes in mesophyll diffusion conductance and photosynthetic capacity under different light and water availabilities in *Populus tremula*: how structure constrains function, Plant Cell Environ, 35 (2012) 839-856.

[15] M. Tomas, J. Flexas, L. Copolovici, J. Galmes, L. Hallik, H. Medrano, M. Ribas-Carbo, T. Tosens, V. Vislap, U. Niinemets, Importance of leaf anatomy in determining mesophyll diffusion conductance to CO_2 across species: quantitative limitations and scaling up by models, J Exp Bot, 64 (2013) 2269-2281.

[16] T.D. Sharkey, Photosynthesis in intact leaves of C_3 plants - physics, physiology and rate limitations, Bot Rev, 51 (1985) 53-105.

[17] J. Flexas, A. Diaz-Espejo, J.A. Berry, J. Cifre, J. Galmes, R. Kaidenhoff, H. Medrano, M. Ribas-Carbo, Analysis of leakage in IRGA's leaf chambers of open gas exchange systems: quantification and its effects in photosynthesis parameterization, J Exp Bot, 58 (2007) 1533-1543.

[18] B. Genty, J.M. Briantais, N.R. Baker, The relationship between the quantum yield of photosynthetic electron-transport and quenching of chlorophyll fluorescence, Biochim Biophys Acta, 990 (1989) 87-92.

[19] A.R. Spurr, A low-viscosity epoxy resin embedding medium for electron microscopy, J Ultra Mol Struct R, 26 (1969) 31-&.

[20] H.K. Mebatsion, P. Verboven, B.E. Verlinden, Q.T. Ho, T.A. Nguyen, B.M. Nicolai, Microscale modelling of fruit tissue using Voronoi tessellations, Comput Electron Agr, 52 (2006) 36-48.

[21] J.F. Thain, Curvature correction factors in the measurement of cell-surface areas in plant-tissues, J Exp Bot, 34 (1983) 87-94.

[22] J.R. Evans, S. Von Caemmerer, B.A. Setchell, G.S. Hudson, The relationship between CO2 transfer conductance and leaf Anatomy in transgenic tobacco with a reduced content of Rubisco, Aust J Plant Physiol, 21 (1994) 475-495.

[23] J. Galmes, J.M. Ochogavia, J. Gago, E.J. Roldan, J. Cifre, M.A. Conesa, Leaf responses to drought stress in Mediterranean accessions of *Solanum lycopersicum*: anatomical adaptations in relation to gas exchange parameters, Plant Cell Environ, 36 (2013) 920-935.

[24] U. Niinemets, M. Reichstein, Controls on the emission of plant volatiles through stomata: A sensitivity analysis, J Geophys Res-Atmos, 108 (2003).

[25] D. Tholen, X.G. Zhu, The mechanistic basis of internal conductance: a Theoretical analysis of mesophyll cell photosynthesis and CO2 diffusion, Plant Physiol, 156 (2011) 90-105.

[26] Q.T. Ho, H.N.C. Berghuijs, R. Watté, P. Verboven, E. Herremans, X. Yin, M.A. Retta, B. Aernouts, W. Saeys, L. Helfen, G.D. Farquhar, P.C. Struik, B.M. Nicolai, 2015. 3-D microscale modeling of CO_2 transport and light propagation in tomato leaves enlightens photosynthesis, Plant Cell Environ., in press.

[27] S.W. Fanta, W. Vanderlinden, M.K. Abera, P. Verboven, R. Karki, Q.T. Ho, S. De Feyter, J. Carmeliet, B.M. Nicolai, Water transport properties of artificial cell walls, J Food Eng, 108 (2012) 393-402.

[28] S. von Caemmerer, R.T. Furbank, The C_4 pathway: an efficient CO_2 pump, Photosynth Res, 77 (2003) 191-207.

[29] J.R. Evans, R. Kaldenhoff, B. Genty, I. Terashima, Resistances along the CO_2 diffusion pathway inside leaves, J Exp Bot, 60 (2009) 2235-2248.

[30] J. Gutknecht, M.A. Bisson, F.C. Tosteson, Diffusion of carbon-dioxide through lipid bilayer membranes - effects of carbonic-anhydrase, Bicarbonate, and Unstirred Layers, J Gen Physiol, 69 (1977) 779-794.

[31] I. Terashima, Y.T. Hanba, Y. Tazoe, P. Vyas, S. Yano, Irradiance and phenotype: comparative eco-development of sun and shade leaves in relation to photosynthetic CO_2 diffusion, J Exp Bot, 57 (2006) 343-354.

[32] D. Tholen, C. Boom, X.G. Zhu, Opinion: Prospects for improving photosynthesis by altering leaf anatomy, Plant Sci, 197 (2012) 92-101.

[33] Q.T. Ho, P. Verboven, X. Yin, P.C. Struik, B.M. Nicolai, A Microscale model for combined CO_2 Diffusion and photosynthesis in leaves, Plos One, 7 (2012).

[34] T. Aalto, E. Juurola, A three-dimensional model of CO2 transport in airspaces and mesophyll cells of a silver birch leaf, Plant Cell Environ, 25 (2002) 1399-1409.

[35] D.F. Parkhurst, 3-Dimensional Model for CO_2 uptake by continuously distributed mesophyll in leaves, J Theor Biol, 67 (1977) 471-488.

[36] N. Uehlein, B. Otto, D.T. Hanson, M. Fischer, N. McDowell, R. Kaldenhoff, Function of Nicotiana tabacum aquaporins as chloroplast gas pores challenges the concept of membrane CO_2 permeability, Plant Cell, 20 (2008) 648-657.

[37] P. Verboven, E. Herremans, L. Helfen, Q.T. Ho, M. Abera, T. Baumbach, M. Wevers, B.M. Nicolai, Synchrotron X-ray computed laminography of the three-dimensional anatomy of tomato leaves, Plant J, 81 (2015) 169-182.

[38] D.F. Parkhurst, Diffusion of CO_2 and other gases inside leaves, New Phytol, 126 (1994) 449-479.

[39] J. Flexas, M.M. Barbour, O. Brendel, H.M. Cabrera, M. Carriqui, A. Diaz-Espejo, C. Douthe, E. Dreyerc, J.P. Ferrio, J. Gago, A. Galle, J. Galmes, N. Kodama, H. Medrano, U. Niinemets, J.J. Peguero-Pina, A. Poua, M. Ribas-Carbo, M. Tomas, T. Tosens, C.R. Warren, Mesophyll diffusion conductance to CO_2: An unappreciated central player in photosynthesis (vol 193, pg 70, 2012), Plant Sci, 196 (2012) 31-31.

[40] I. Terashima, Y.T. Hanba, D. Tholen, U. Niinemets, Leaf functional anatomy in relation to photosynthesis, Plant Physiol, 155 (2011) 108-116.

[41] G.D. Price, S. Von Caemmerer, J.R. Evans, J.W. Yu, J. Lloyd, V. Oja, P. Kell, K. Harrison, A. Gallagher, M.R. Badger, Specific reduction of chloroplast carbonic-anhydrase activity by antisense RNA in transgenic tobacco plants has a minor effect on photosynthetic CO_2 assimilation, Planta, 193 (1994) 331-340.

[42] T.G. Williams, L.B. Flanagan, J.R. Coleman, Photosynthetic gas exchange and discrimination against (CO_2)-C-13 and (COO)-O-18-O-16 in tobacco plants modified by an antisense construct to have low chloroplastic carbonic anhydrase, Plant Physiol, 112 (1996) 319-326.

[43] J.S. Gillon, D. Yakir, Internal conductance to CO_2 diffusion and (COO)-O-18 discrimination in C_3 leaves, Plant Physiol, 123 (2000) 201-213.

Tables

Table 1. List of variables and their units

Variable	Definition	Unit
A_{N}	Net rate of CO_2 assimilation	$\mu\mathrm{mol\ CO_2\ m^{-2}\ leaf\ s^{-1}}$
C_{a}	CO_2 partial pressure in the atmosphere	$\mu\mathrm{bar\ CO_2}$
C_{i}	CO_2 partial pressure in the stomatal cavity	$\mu\mathrm{bar\ CO_2}$
C_{i0}	CO_2 partial pressure in the stomatal cavity if $I_{\mathrm{inc}} = 0$	$\mu\mathrm{bar\ CO_2}$
C_{c}	CO_2 partial pressure near Rubisco	$\mu\mathrm{bar\ CO_2}$
$D_{\mathrm{CO_2,i}}$	Diffusion coefficient of CO_2 in component i	$\mathrm{m^2\ s^{-1}}$
$D_{\mathrm{CO_2,water}}$	Diffusion coefficient of CO_2 in water	$\mathrm{m^2\ s^{-1}}$
f_{i}	Fraction of the diffusive path length of component i and its thickness	-
f_{pal}	Fraction of the exposed mesophyll surface area that belongs to the palisade parenchyma	-
F	Rate of photorespiratory CO_2 release	$\mu\mathrm{mol\ CO_2\ m^{-2}\ leaf\ s^{-1}}$
G_{mem}	Permeability of the cell wall	$\mathrm{m\ s^{-1}}$
G_{env}	Permeability of the chloroplast envelope	$\mathrm{m\ s^{-1}}$
H	Henry's law constant for CO_2	$\mathrm{Pa\ m^{-3}\ mol^{-1}}$
I_{inc}	Irradiance incident at the leaf surface	$\mu\mathrm{mol\ photons\ m^{-2}\ leaf\ s^{-1}}$
J	Rate of electron transport through Photosystem II	$\mu\mathrm{mol\ e^-\ m^{-2}\ leaf\ s^{-1}}$
J_{max}	Maximum rate of electron transport through Photosystem II at saturating light	$\mu\mathrm{mol\ e^-\ m^{-2}\ leaf\ s^{-1}}$
K_{mC}	Michaelis-Menten constant of Rubisco for CO_2	$\mu\mathrm{bar\ CO_2}$
K_{mO}	Michaelis-Menten constant of Rubisco for O_2	$\mathrm{mbar\ O_2}$
L_{i}	Diffusion path length of component i	m
$\left(\frac{L_{\mathrm{m}}}{L}\right)_{\mathrm{tissue}}$	Fraction of exposed mesophyll length relative to the width of the section at one side of the leaf in a certain tissue (either palisade parenchyma or spongy parenchyma)	$\mathrm{m\ m^{-1}}$
O	O_2 partial pressure	$\mathrm{mbar\ O_2}$
$p_{\mathrm{eff,i}}$	Effective porosity of component i	-
q	Power in the power law that describes the empirical relationship between C_{i} and I_{inc}	
r_{i}	Resistance for CO_2 transport of component i in the mesophyll	$\mathrm{m^2\ leaf\ s\ bar\ CO_2\ mol^{-1}\ CO_2}$
r_{chl}	Lumped resistance for CO_2 transport of the chloroplast envelope and the stroma, and half the resistance of the cytosol	$\mathrm{m^2\ leaf\ s\ bar\ CO_2\ mol^{-1}\ CO_2}$
r_{diff}	Total resistance for CO_2 transport of the physical barriers in the mesophyll	$\mathrm{m^2\ leaf\ s\ bar\ CO_2\ mol^{-1}\ CO_2}$
r_{m}	Apparent mesophyll resistance	$\mathrm{m^2\ leaf\ s\ bar\ CO_2\ mol^{-1}\ CO_2}$
r_{wp}	Lumped resistance for CO_2 transport of the cell wall, the plasma membrane, and half the resistance of the cytosol	$\mathrm{m^2\ leaf\ s\ bar\ CO_2\ mol^{-1}\ CO_2}$

R	Universal gas constant	$\mathrm{J\ K^{-1}\ mol^{-1}}$
R_d	Rate of mitochondrial respiration in the light	$\mathrm{\mu mol\ CO_2\ m^{-2}\ leaf\ s^{-1}}$
R_i	Resistance for CO_2 transport of component i in the mesophyll	$\mathrm{s\ m^{-1}}$
s	Slope of the assumed linear relationship between A_N and $\frac{1}{4} I_\mathrm{inc} \Phi_2$ under strictly electron-transport-limited conditions	-
$\frac{S_\mathrm{c}}{S}$	Fraction of the exposed chloroplast surface area of the palisade parenchyma and the spongy parenchyma relative to leaf surface area at one side of the leaf	$\mathrm{m^2\ chloroplast\ m^{-2}\ leaf}$
$\frac{S_\mathrm{c}}{S_\mathrm{m}}$	Fraction of the exposed chloroplast surface area of the palisade parenchyma and the spongy parenchyma relative to the exposed mesophyll surface area of these tissues	$\mathrm{m^2\ chloroplast\ m^{-2}\ mesophyll}$
$S_\mathrm{C/O}$	Relative CO_2/O_2 specificity factor of Rubisco	$\mathrm{mbar\ O_2\ \mu bar^{-1}\ CO_2}$
$\frac{S_\mathrm{m}}{S}$	Fraction of the exposed mesophyll surface area of the palisade parenchyma and the spongy parenchyma relative to leaf surface area at one side of the leaf	$\mathrm{m^2\ mesophyll\ m^{-2}\ leaf}$
t_i	Weighted average thickness of a mesophyll component i in the palisade and the spongy parenchyma	m
T	Temperature	K
T_p	Rate of triose phosphate utilization	$\mathrm{\mu mol\ phosphate\ m^{-2}\ leaf\ s^{-1}}$
α_2LL	Quantum yield of electron transport through Photosystem II under strictly electron-transport-limiting conditions on the basis of light absorbed by both Photosystem I and Photosystem II	$\mathrm{mol\ e^-\ mol^{-1}\ photon}$
γ_tissue	Curvature factor of a certain tissue (either palisade parenchyma or spongy parenchyma)	-
Γ^*	CO_2 compensation point	$\mathrm{\mu bar\ CO_2}$
θ	Convexity factor of the response of J to I_inc	-
ζ_i	Reduction factor of the diffusion coefficient of CO_2 relative to $D_{\mathrm{CO_2,water}}$ in component i due to the higher viscosity of i	
κ_2LL	Conversion factor of incident irradiance into electron transport under electron-transport-limited conditions	$\mathrm{mol\ e^-\ mol^{-1}\ photon}$
Φ_2	Quantum yield of electron transport through Photosystem II	$\mathrm{mol\ e^-\ mol^{-1} photon}$
ω	Ratio of r_chl to r_diff	-

1

2

Table 2. Measurements of the ratio of $\frac{S_c}{S}$ for each cultivar (Admiro, Doloress, Growdena), leaf age (15 days and 25 days after appearance) and tissue type (palisade parenchyma and spongy parenchyma and total mesophyll).

Cultivar	Leaf age (days)	Tissue type	$\frac{S_{\mathrm{m}}}{S}$	$\frac{L_c}{L_{\mathrm{m}}}$	$\frac{S_{\mathrm{c}}}{S}$
Admiro	15	pal[1]	8.99	0.96	8.66
		spo[2]	8.04	0.87	7.00
		mes[3]	17.04		15.66
	25	pal	8.29	0.98	8.09
		spo	8.31	0.84	6.96
		mes	16.61		15.05
Doloress	15	pal	8.29	0.94	7.87
		spo	8.94	0.95	8.51
		mes	17.23		16.38
	25	pal	8.37	0.96	8.00
		spo	9.04	0.90	8.13
		mes	17.41		16.13
Growdena	15	pal	8.70	0.94	8.14
		spo	8.91	0.87	7.81
		mes	17.64		15.96
	25	pal	7.29	0.90	6.55
		spo	8.97	0.87	7.78
		mes	16.26		14.34

[1] pal: palisade parenchyma
[2] spo: spongy parenchyma
[3] mes: whole mesophyll

1

Table 3. Average thicknesses (± the standard errors of the mean) of the cell wall, cytosol and stroma for all studied cultivars (Admiro, Doloress, Growdena), leaf ages (15 days and 25 days after emergence) and tissue types (palisade and spongy parenchyma and total mesophyll).

			Component thickness (µm)		
Cultivar	Leaf age (days)	Tissue type	Cell wall	Cytosol	Stroma
Admiro	15	pal[1]	0.120 ± 0.006[5]	0.256 ± 0.036	2.691 ± 0.211
		spo[2]	0.117 ± 0.010	0.229 ± 0.019	2.366 ± 0.186
		mes[3,4]	0.119	0.243	2.55
	25	pal	0.168 ± 0.020	0.257 ± 0.035	2.273 ± 0.153
		spo	0.170 ± 0.022	0.235 ± 0.021	2.613 ± 0.771
		mes	0.169	0.246	2.43
Doloress	15	pal	0.104 ± 0.008	0.172 ± 0.023	2.691 ± 0.394
		spo	0.151 ± 0.026	0.263 ± 0.042	2.577 ± 0.571
		mes	0.128	0.212	2.63
	25	pal	0.146 ± 0.008	0.184 ± 0.027	2.552 ± 0.633
		spo	0.145 ± 0.015	0.269 ± 0.044	2.213 ± 0.340
		mes	0.145	0.231	2.38
Growdena	15	pal	0.089 ± 0.005	0.194 ± 0.041	2.218 ± 0.266
		spo	0.125 ± 0.009	0.304 ± 0.098	2.035 ± 0.158
		mes	0.107	0.250	2.13
	25	pal	0.177 ± 0.022	0.404 ± 0.098	2.708 ± 0.691
		spo	0.208 ± 0.023	0.492 ± 0.093	2.550 ± 0.356
		mes	0.193	0.453	2.62

[1] pal: palisade parenchyma
[2] spo: spongy parenchyma
[3] mes: total mesophyll
[4] The values represent the weighted average thicknesses of these compartments in the palisade and the spongy parenchyma.
[5] standard error of the mean

1

2

3

Table 4. Values for ω and r_{diff} calculated for each cultivar (Admiro, Doloress, Growdena) and leaf age (15 days and 25 days after leaf appearance)

Cultivar	Leaf age (days)	ω	r_{diff} ($\mathrm{m^2\ s\ bar\ mol^{-1}}$)
Admiro	15	0.67	3.94
	25	0.63	4.27
Doloress	15	0.66	3.85
	25	0.64	3.86
Growdena	15	0.66	3.59
	25	0.62	5.09

Table 5. Maximum difference in A_{N} and the corresponding C_{i} in simulated $A - C_{\mathrm{i}}$ curves, if a parameter ϱ is 25% increased or decreased.

Parameter	$\max(\Delta A_{\mathrm{n}})$ $\varrho = (1-0.25)\varrho_{\mathrm{default}}$ [1]		$\max(\Delta A_{\mathrm{n}})$ $\varrho = (1+0.25)\varrho_{\mathrm{default}}$	
	C_{i}	ΔA_{N}	C_{i}	ΔA_{N}
$\frac{L_{\mathrm{m}}}{L}$ [2]	245	-4.97	218	3.47
$\frac{L_{\mathrm{c}}}{L_{\mathrm{m}}}$ [3]	245	-3.63	- [4]	- [4]
t_{wall}	241	0.335	245	-0.457
t_{cyt}	241	0.481	245	-0.474
t_{str}	234	1.65	245	-1.59
p_{eff}	245	-0.605	241	0.370
G_{mem}	245	-0.524	241	0.319
ζ_{cyt}	245	-0.629	241	0.383
G_{env}	245	-1.70	238	1.06
ζ_{str}	245	-2.09	234	1.32
f_{str}	234	-1.64	245	-1.59
γ_{pal}	245	-2.46	226	2.02
γ_{spo}	245	-2.17	230	1.81

[1] ϱ denotes the parameter which was varied. $\varrho_{\mathrm{default}}$ denotes the default value of this parameter.

[2] Both $\left(\frac{L_{\mathrm{m}}}{L}\right)_{\mathrm{pal}}$ and $\left(\frac{L_{\mathrm{m}}}{L}\right)_{\mathrm{spo}}$ were respectively decreased or increased by 25%.

[3] Both $\left(\frac{L_{\mathrm{c}}}{L_{\mathrm{m}}}\right)_{\mathrm{pal}}$ and $\left(\frac{L_{\mathrm{c}}}{L_{\mathrm{m}}}\right)_{\mathrm{spo}}$ were respectively decreased or increased by 25%.

[4] Since $\left(\frac{L_{\mathrm{c}}}{L_{\mathrm{m}}}\right)_{\mathrm{pal}}$ and $\left(\frac{L_{\mathrm{c}}}{L_{\mathrm{m}}}\right)_{\mathrm{spo}}$ cannot be larger than 1, we did not increase this parameter by 25%.

Table 6. Maximum difference in A_{N} and the corresponding C_{i} in simulated $A - I_{\mathrm{inc}}$ curves (in all cases $I_{\mathrm{inc}} = 1500\ \mu\mathrm{mol\ m^{-2}\ s^{-1}}$), if a parameter ϱ is 25% increased or decreased.

Parameter	$\max(\Delta A_{\mathrm{n}})$ $\varrho = (1-0.25)\varrho_{\mathrm{default}}$ [1]	$\max(\Delta A_{\mathrm{n}})$ $\varrho = (1+0.25)\varrho_{\mathrm{default}}$ [1]
	ΔA_{N}	ΔA_{N}
$\frac{L_{\mathrm{m}}}{L}$ [2]	-4.91	2.94
$\frac{L_{\mathrm{c}}}{L_{\mathrm{m}}}$ [3]	-3.59	- [4]
t_{wall}	0.466	-0.449
t_{cyt}	0.479	-0.470
t_{str}	1.44	-1.57
p_{eff}	-0.595	0.371
G_{mem}	-0.515	0.319
ζ_{cyt}	-0.621	0.384
G_{env}	-1.68	0.960
ζ_{str}	-2.07	1.17
f_{str}	1.44	-1.57
γ_{pal}	-2.43	1.76
γ_{spo}	-2.14	1.59

[1] ϱ denotes the parameter which was varied. $\varrho_{\mathrm{default}}$ denotes the default value of this parameter.

[2] Both $\left(\frac{L_{\mathrm{m}}}{L}\right)_{\mathrm{pal}}$ and $\left(\frac{L_{\mathrm{m}}}{L}\right)_{\mathrm{spo}}$ were respectively decreased or increased by 25%.

[3] Both $\left(\frac{L_{\mathrm{c}}}{L_{\mathrm{m}}}\right)_{\mathrm{pal}}$ and $\left(\frac{L_{\mathrm{c}}}{L_{\mathrm{m}}}\right)_{\mathrm{spo}}$ were respectively decreased or increased by 25%.

[4] Since $\left(\frac{L_{\mathrm{c}}}{L_{\mathrm{m}}}\right)_{\mathrm{pal}}$ and $\left(\frac{L_{\mathrm{c}}}{L_{\mathrm{m}}}\right)_{\mathrm{spo}}$ cannot be larger than 1, we did not increase this parameter by 25%.

1

2

Figures

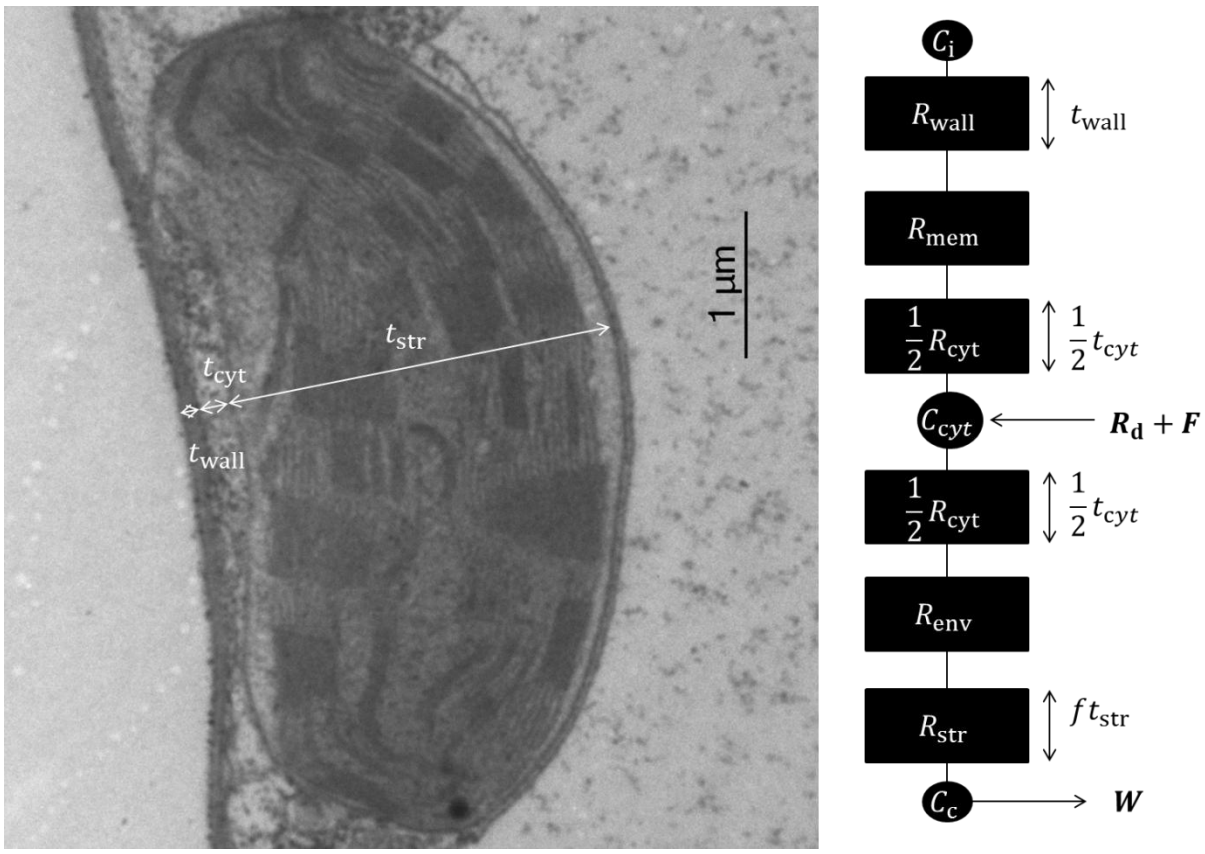

a) **b)**

Figure 1:

a): Sample TEM image. A single chloroplast in the palisade parenchyma in a 25-day-old *S. lycopersicum* L. cv. Admiro leaf. The double arrows represent the thicknesses of the cell wall t_{wall}, the cytosol t_{cyt} and the chloroplast t_{str}.

b): Schematic representation of the resistance model used in this study. The circles represent CO_2 partial pressures in the intercellular airspaces (C_i), in the middle of the cytosol (C_{cyt}) and in the stroma near Rubisco (C_c). The boxes represent the resistances of the cell wall (R_{wall}), the plasma membrane (R_{mem}), the two compartments of the cytosol (R_{cyt}), the chloroplast envelope (R_{env}) and the stroma (R_{str}). The double arrows show the assumed thickness of the resistances of the cell wall, the cytosol and the stroma. The single arrows show the CO_2 sink (rate of CO_2 carboxylation W) and the sources (rate of mitochondrial respiration in the light R_d and the rate of photorespiration F.

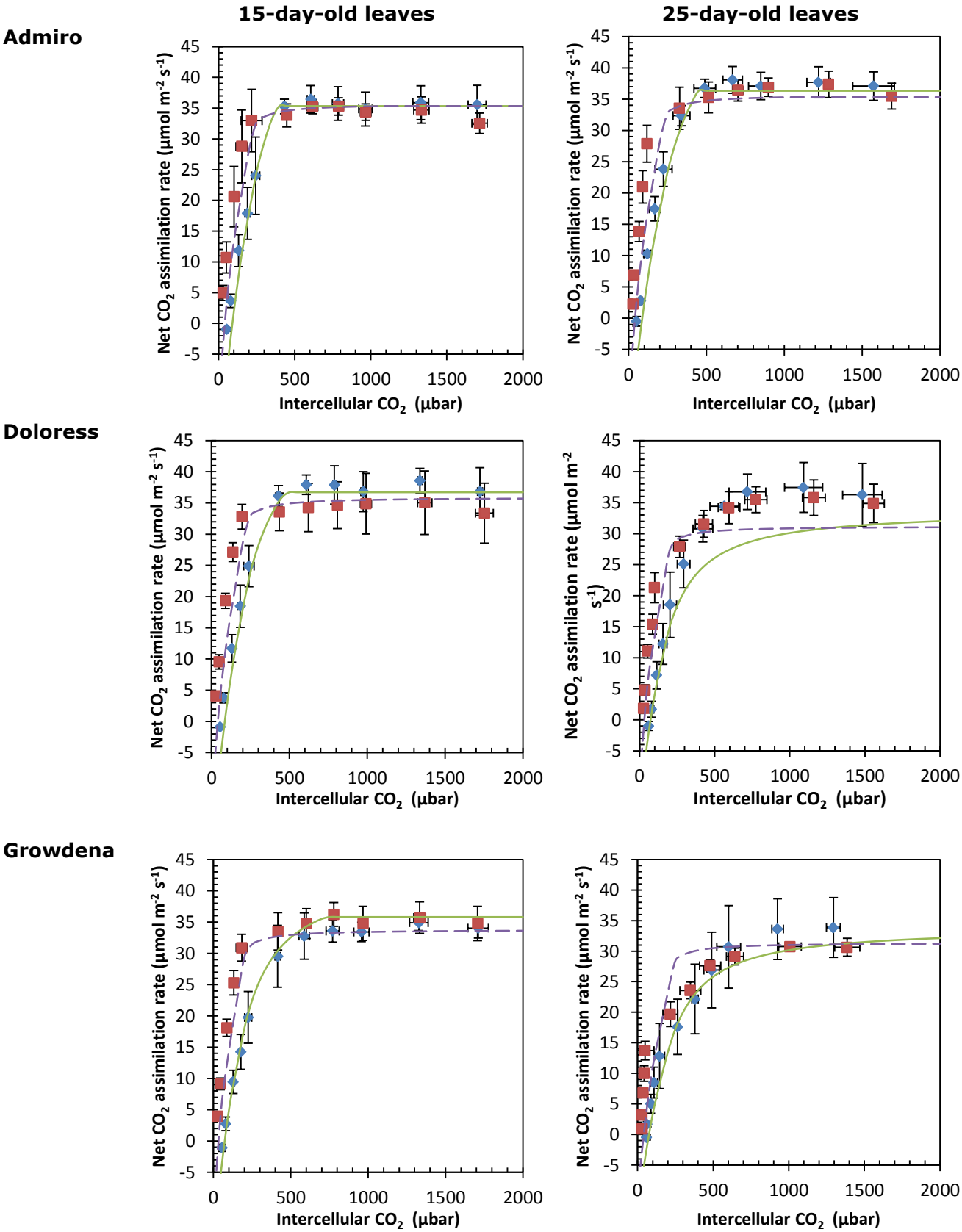

Figure 2: Measured and simulated CO_2 response curves at saturating light ($I_{inc} = 1500\ \mu mol\ m^{-2}\ s^{-1}$). Measured rates of net CO_2 assimilation at $O = 210$ mbar (diamonds±one standard error) and at $O = 20$ mbar and (squares±one standard error) for three cultivars (Admiro, Doloress, Growdena) and two leaf ages (15 days and 25 days after emergence). Simulated rates of net CO_2 assimilation at $O = 210$ mbar (solid lines) and at $O = 20$ mbar (squares).

1

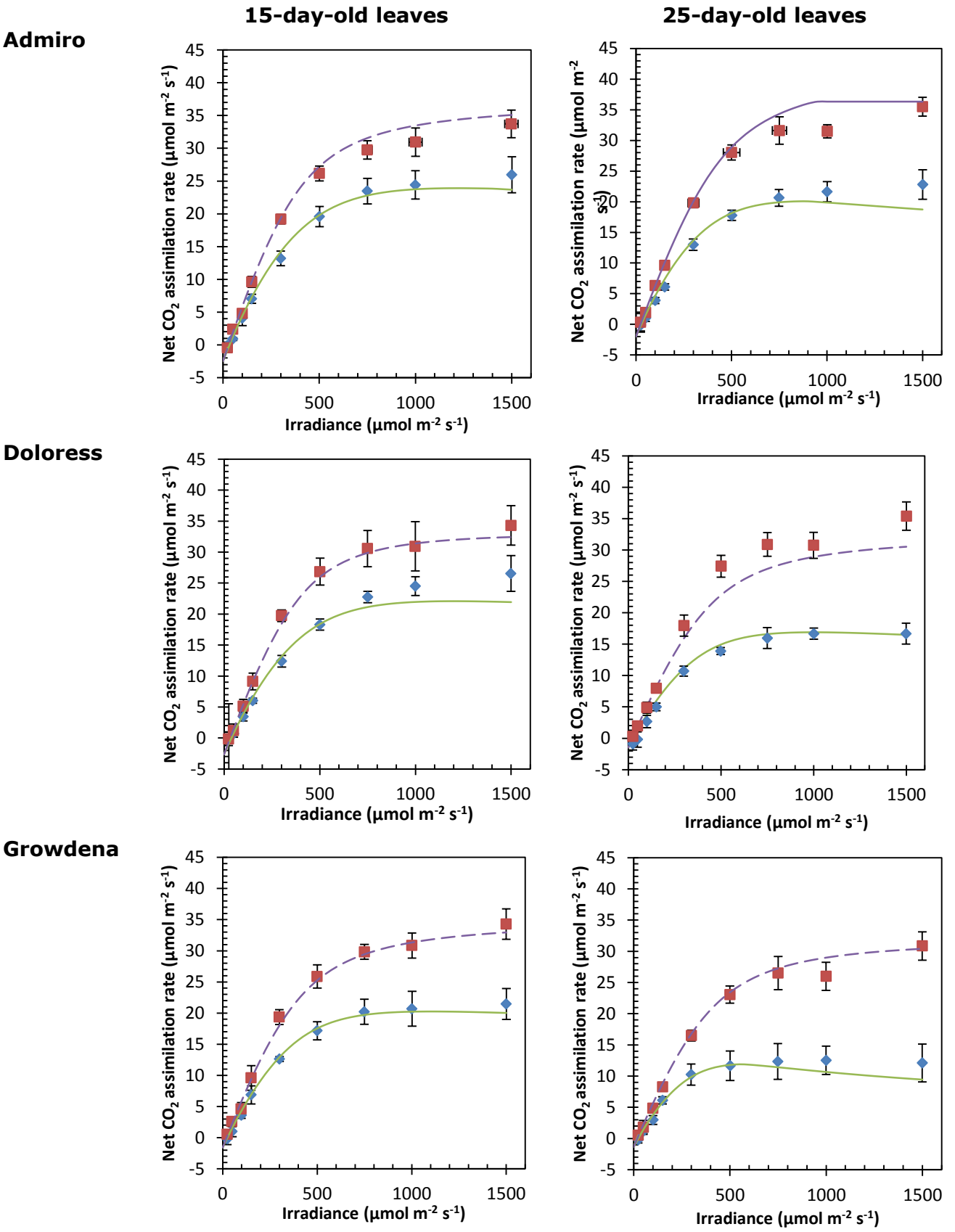

Figure 3: Measured and simulated light response curves. Measured rates of net CO_2 assimilation at $O = 210$ mbar and $C_a = 400$ µbar (diamonds±one standard error) and at $O = 20$ mbar and $C_a = 1000$ µbar (squares±one standard error) for three cultivars (Admiro, Doloress, Growdena) and two leaf ages (15 days and 25 days after emergence). Simulated rates of net CO_2 assimilation at $O = 210$ mbar and $C_a = 400$ µbar (solid lines) and at $O = 20$ mbar and $C_a = 1000$ µbar (squares).

1

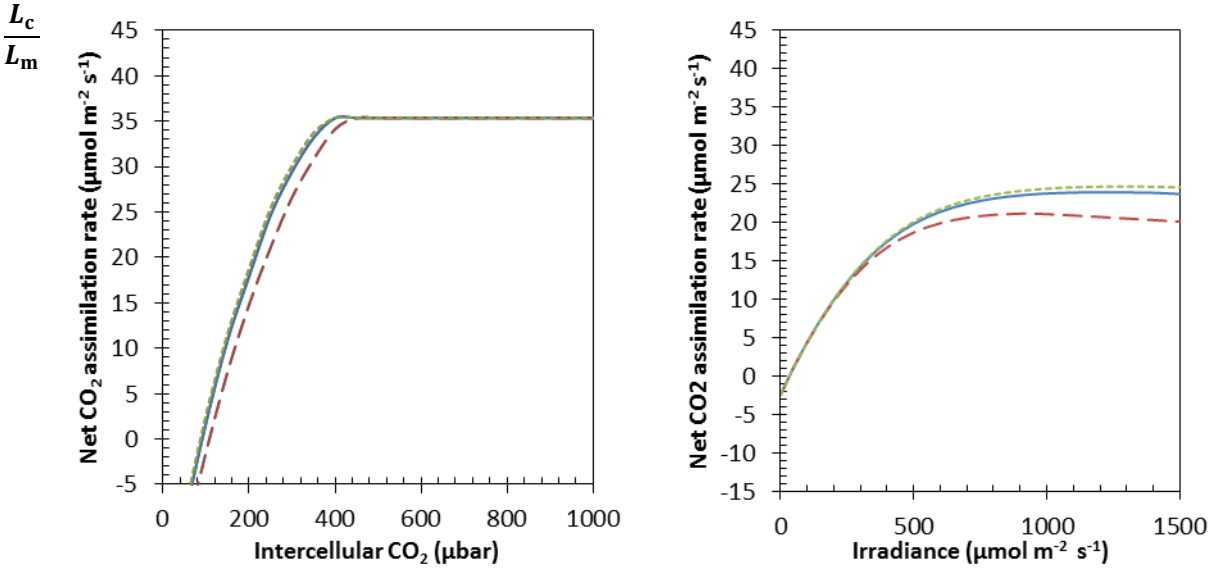

Figure 4: Sensitivity analysis $A - C_i$ curve and $A - I_{inc}$ curve for $\frac{L_c}{L_m}$. Parameter $\frac{L_c}{L_m}$ of the model is either decreased by 25% (dashed line) or set to 1 (short dashed line). The continuous line represents the simulated $A - C_i$ curve for default parameter values.

1

2

1

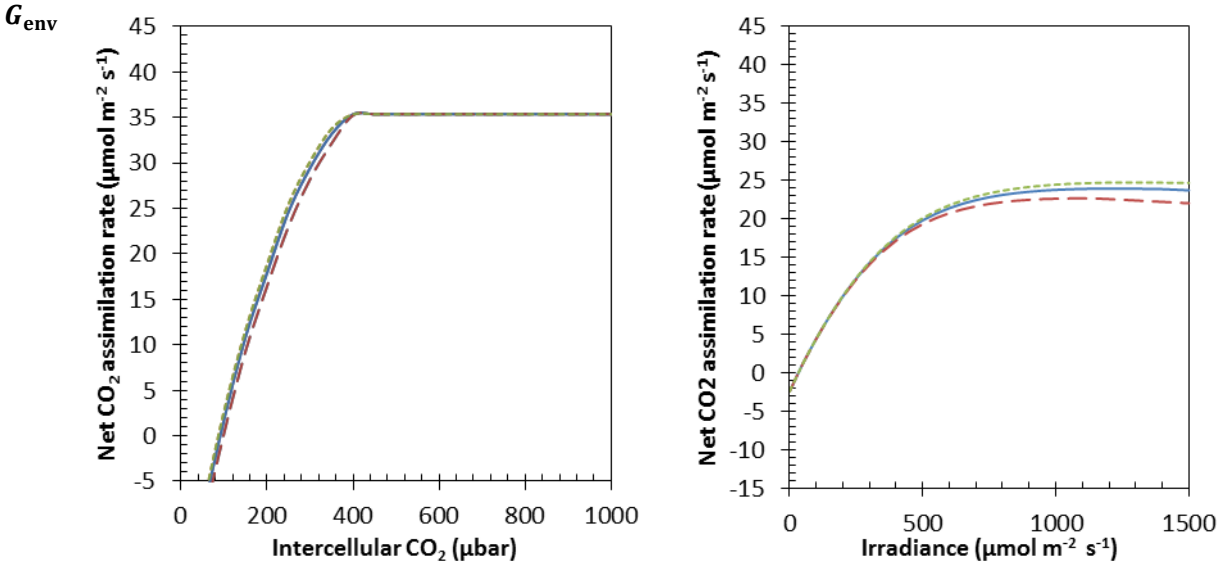

Figure 5: Sensitivity analysis $A - C_{\mathrm{i}}$ curve and $A - I_{\mathrm{inc}}$ curve for G_{env}. Parameter $\frac{L_{\mathrm{c}}}{L_{\mathrm{m}}}$ of the model is either decreased by 25% (dashed line) or increased by 25% (short dashed line). The continuous line represents the simulated $A - C_{\mathrm{i}}$ curve for default parameter values.

2

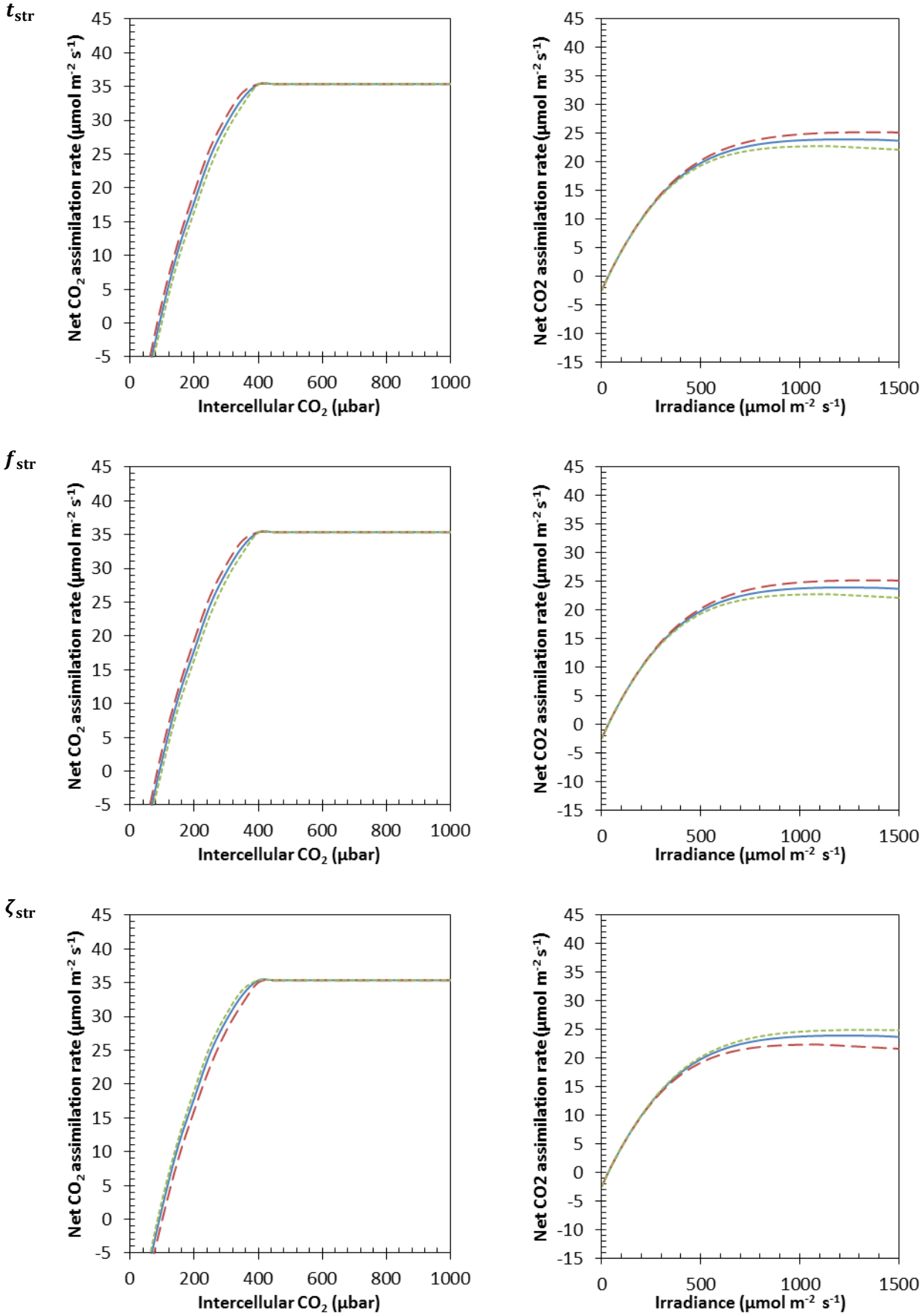

Figure 6: Sensitivity analysis $A - C_i$ curves and $A - I_{inc}$ curves for t_{str}, f_{str} and ζ_{str}. Model parameters are either decreased by 25% (long dashed line) or increased by 25 (short dashed line). The continuous line represents the simulated $A - C_i$ curve for default parameter values.

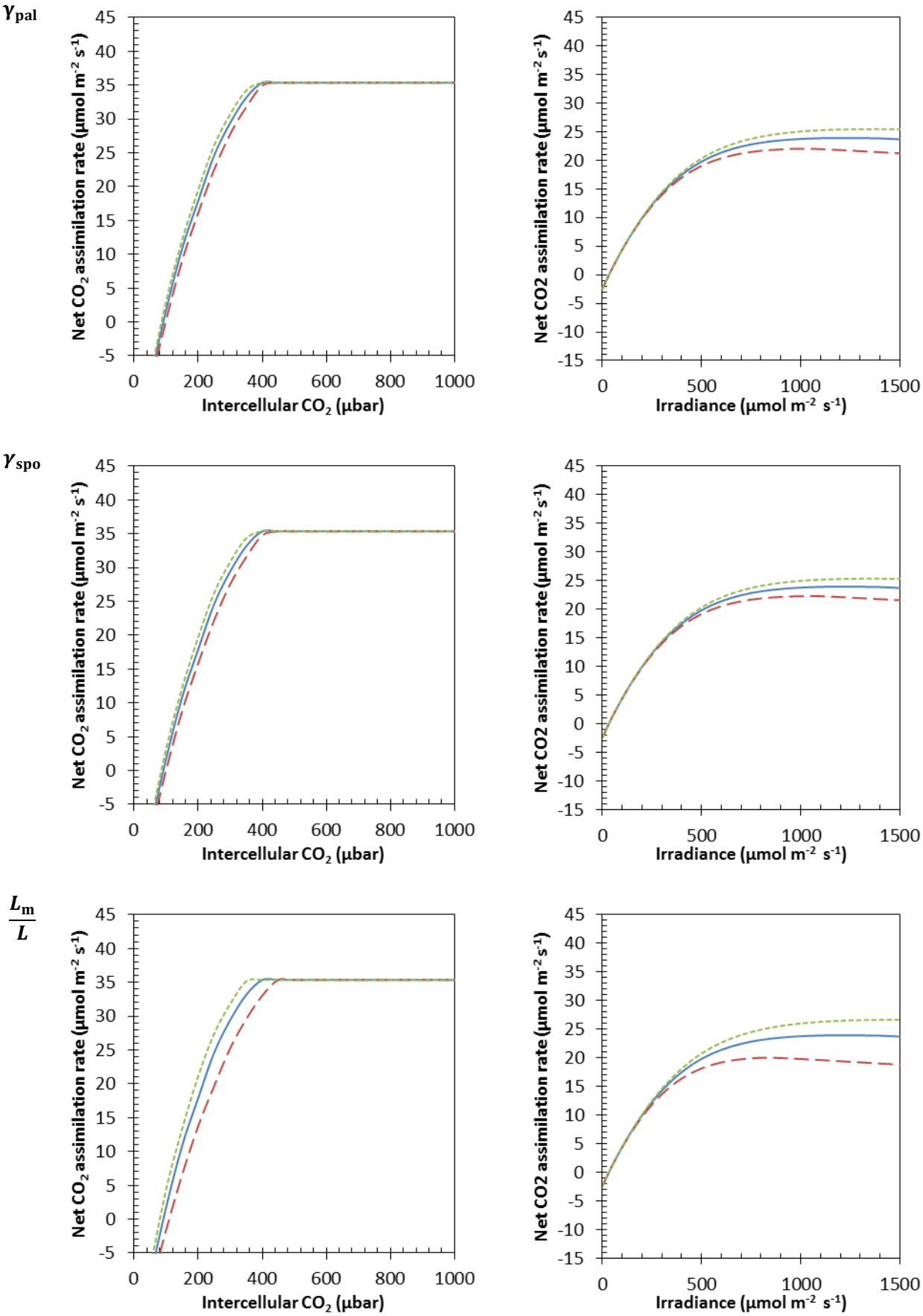

Figure 7: Sensitivity analysis $A - C_i$ curves and $A - I_{inc}$ curve for γ_{pal},γ_{spo} and $\frac{L_m}{L}$. Model parameters are either decreased by 25% (long dashed line) or increased by 25 (short dashed line). The continuous line represents the simulated $A - C_i$ curve for default parameter values.

1